Radiology

Detection of Small Pulmonary Nodules with Ultrashort Echo Time Sequences in Oncology Patients by Using a PET/MR System[1]

Nicholas S. Burris, MD
Kevin M. Johnson, PhD
Peder E. Z. Larson, PhD
Michael D. Hope, MD
Scott K. Nagle, MD, PhD
Spencer C. Behr, MD
Thomas A. Hope, MD

Purpose: To investigate the utility of a free-breathing ultrashort echo time (UTE) sequence for the evaluation of small pulmonary nodules in oncology patients by using a hybrid positron emission tomography (PET)/magnetic resonance (MR) imaging system and to compare the nodule detection rate between UTE and a conventional three-dimensional gradient-recalled-echo (GRE) technique.

Materials and Methods: In this HIPAA-compliant, institutional review board–approved prospective study, 82 pulmonary nodules were identified in eight patients with extrathoracic malignancies. Patients underwent free-breathing UTE and dual-echo three-dimensional GRE imaging of the lungs in a hybrid PET/MR imaging unit immediately after clinical PET/computed tomography (CT). CT was considered the reference standard for nodule detection. Two reviewers identified nodules and obtained measurements on MR images. The McNemar test was used to evaluate differences in nodule detection rate between MR techniques, and interrater agreement was assessed by using Bland-Altman plots.

Results: Mean nodule diameter ± standard deviation was 6.2 mm ± 2.7 (range, 3–17 mm). The detection rate was higher for UTE imaging than for dual-echo GRE imaging for nodules of at least 4 mm (82% vs 34%, respectively; $P < .001$), with the largest difference in detection noted in the 4–8-mm nodule group (79% vs 21%, $P < .001$). UTE imaging displayed a higher detection rate than dual-echo GRE imaging for nodules without fluorodeoxyglucose avidity (68% vs 22%, respectively; $P < .001$). Interrater reliability of nodule detection with MR imaging was high ($\kappa = 0.90$ for UTE imaging and $\kappa = 0.92$ for dual-echo GRE imaging).

Conclusion: A free-breathing UTE sequence has high sensitivity for the detection of small pulmonary nodules (4–8 mm) and outperformed a three-dimensional dual-echo GRE technique for the detection of small, non–fluorodeoxyglucose-avid nodules.

[1] From the Department of Radiology (N.S.B., P.E.Z.L., M.D.H., S.C.B., T.A.H.), University of California–San Francisco, 505 Parnassus Ave, Box 0628, San Francisco, CA 94143-0628; Departments of Medical Physics (K.M.J., S.K.N.), Radiology (S.K.N.), and Pediatrics (S.K.N.), University of Wisconsin, Madison, Wis; and UCSF Graduate Program in Bioengineering, University of California–Berkeley, Berkeley, Calif (P.E.Z.L.). Received February 26, 2015; revision requested March 31; revision received April 10; accepted April 29; final version accepted May 6. S.C.B. and T.A.H. supported by GE Healthcare. **Address correspondence to** T.A.H. (e-mail: *thomas.hope@ucsf.edu*).

Recent advances in multimodality imaging technology have allowed for simultaneous magnetic resonance (MR) imaging and positron emission tomography (PET) acquisition. While hybrid PET/MR imaging systems are now available (1), poor evaluation of the lung parenchyma remains a substantial limitation to the widespread clinical implementation of these systems. The MR imaging detection rate of large pulmonary nodules (>1 cm) is high; however, the detection rate of subcentimeter nodules remains inadequate for routine clinical evaluation (2–4). Nodules smaller than 5 mm in diameter are unlikely to be malignant in any patient population (5,6). However, in patients with known malignancy, it is important to detect nodules with 5–10-mm diameters, particularly in the setting of melanoma, sarcoma, or testicular carcinoma, which have high rates of pulmonary nodule malignancy (5,7,8). Improved detection of these small pulmonary nodules would increase the feasibility of stand-alone PET/MR imaging for clinical staging and surveillance in oncology patients.

Pulmonary imaging with MR imaging has traditionally been limited by the low proton density, rapid signal decay, and substantial respiratory and cardiac motion present in lung tissue. Considering the short T2 and T2* values of the lung, a short echo time is an important characteristic of MR imaging sequences used for lung evaluation (9). In previous studies of pulmonary nodule detection with MR imaging, investigators have used fast spin-echo (10), diffusion-weighted (11), ultrafast steady-state free precession (12), zero echo time (13), and three-dimensional (3D) gradient-recalled-echo (GRE) techniques (2,3). Recently, a free-breathing 3D radial ultrashort echo time (UTE) technique has been described for the evaluation of structural lung disease (14). With this technique, a UTE (80-μsec) sequence is used to capture the rapidly decaying lung parenchymal signal (15), adaptive respiratory gating is used to minimize motion artifacts, and variable density readout gradients are used to improve signal-to-noise ratio, resulting in high-spatial-resolution images (1.25-mm isotropic images) acquired with reasonable imaging times (less than 5 minutes). The aim of this study was to investigate the utility of a free-breathing UTE sequence for the evaluation of small pulmonary nodules in oncology patients by using a hybrid PET/MR system and to compare the nodule detection rate between UTE imaging and a conventional 3D GRE technique.

Advances in Knowledge

- A free-breathing ultrashort echo time (UTE) sequence has a high detection rate for pulmonary nodules measuring 4–17 mm (58 of 70 nodules, 83%).
- UTE sequences enabled detection of all fluorodeoxyglucose (FDG)-avid nodules and had a high detection rate for non–FDG-avid pulmonary nodules at least 4 mm in diameter (79%).

Materials and Methods

All procedures were approved by the local institutional review board and were Health Insurance Portability and Accountability Act compliant, and informed consent was obtained from all subjects. Two investigators of this study (T.A.H. and S.C.B.) received research grant support from GE Healthcare; however, the primary investigator and all other authors had full control of the data and information presented in this publication.

Implications for Patient Care

- UTE sequences can be used to identify pulmonary nodules (4–17 mm) in patients with cancer who are undergoing hybrid PET/MR imaging, even in the absence of FDG avidity.
- Detection of pulmonary nodules up to 4 mm in diameter remains limited with MR imaging techniques.

Patients

During a 4-month period (August 2014 through November 2014), we prospectively enrolled eight patients with known pulmonary nodules who were scheduled to undergo PET/computed tomography (CT) for clinical oncologic evaluation. Mean patient age ± standard deviation was 58.6 years ± 13.6 (range, 45–80 years). Most patients were male (five of eight), and men were significantly older than women according to results of the Student *t* test to assume unequal variance (65.4 years ± 11.7 [range, 56–80 years] vs 47.3 years ± 2.1 [range, 45–49 years], respectively; P = .03). The primary malignancy for which the patient was undergoing clinical PET/CT included melanoma (n = 5), breast carcinoma (n = 2), and papillary thyroid carcinoma (n = 1). To maximize the number of small pulmonary nodules available for evaluation, an effort was made to enroll patients with at least two solid pulmonary nodules (ie, not "ground-glass" nodules) smaller than 2 cm in diameter. Patients were excluded on the basis of

Published online before print
10.1148/radiol.2015150489 **Content codes:** CH MR NM

Radiology 2016; 278:239–246

Abbreviations:
FDG = fluorodeoxyglucose
GRE = gradient-recalled echo
UTE = ultrashort echo time
3D = three-dimensional

Author contributions:
Guarantors of integrity of entire study, N.S.B., T.A.H.; study concepts/study design or data acquisition or data analysis/interpretation, all authors; manuscript drafting or manuscript revision for important intellectual content, all authors; approval of final version of submitted manuscript, all authors; agrees to ensure any questions related to the work are appropriately resolved, all authors; literature research, N.S.B., P.E.Z.L., M.D.H., S.C.B., T.A.H.; clinical studies, N.S.B., K.M.J., P.E.Z.L., M.D.H., T.A.H.; experimental studies, N.S.B., K.M.J., P.E.Z.L.; statistical analysis, N.S.B.; and manuscript editing, all authors

Funding:
This research was supported by the National Institutes of Health (grants UL1TR000427, KL2TR000428, and 5T32EB001631-10).

Conflicts of interest are listed at the end of this article.

Table 1

Patient Demographics and Characteristics

Patient No.	Age (y)	Sex	Primary Malignancy	No. of Nodules	Mean Nodule Diameter (mm)*
1	48	Female	Breast	4	3.3 ± 0.3
2	59	Male	Melanoma	3	3.3 ± 0.8
3	53	Male	Papillary thyroid	8	4.9 ± 2.2
4	80	Male	Melanoma	20	6.7 ± 3.3
5	49	Female	Breast	36	7.0 ± 2.1
6	79	Male	Melanoma	3	6.0 ± 2.7
7	45	Female	Melanoma	2	6.0 ± 4.2
8	56	Male	Melanoma	6	5.0 ± 2.3
Mean*	58.6 ± 13.6	…	…	10.3 ± 11.9	6.2 ± 2.6

* Data are means ± standard deviations.

Table 2

Imaging Parameters for Lung MR Imaging Techniques

Imaging Parameter	UTE Sequence	Dual-Echo GRE Sequence
Echo time	80 μsec	1.3 msec out of phase, 2.6 msec in phase
Repetition time (msec)	2.3	5.6
Section thickness (mm)	1.25	3
Voxel size (mm^3)	1.25 × 1.25 × 1.25	1.3 × 0.7 × 3.0
Flip angle (degrees)	4	12
Respiratory gating method	Adaptive bellows	Breath hold
No. of signals acquired	1	0.68
Approximate acquisition time	4 minutes 30 seconds	22 seconds

their history or as a result of preceding clinical PET/CT scanning if they had *(a)* contraindication to MR imaging (eg, pacemaker, metallic foreign bodies, claustrophobia), *(b)* more than small-sized pleural effusion, or *(c)* resolution of previously identified nodules at preceding clinical PET/CT. Clinical and demographic patient information is summarized in Table 1.

Clinical PET/CT Technique

All PET/CT examinations were performed by using a Biograph 16 Hi-Rez PET/CT scanner (Siemens Medical Solutions, Erlangen, Germany) with an integrated PET and 16-section multidetector CT scanner or a Discovery VCT PET/CT scanner (GE Healthcare, Waukesha, Wis) with an integrated PET and 64-section multidetector CT scanner. All patients fasted with hydration for at least 6 hours prior to PET/CT examinations, and blood glucose levels were measured just before fluorodeoxyglucose (FDG) injection and were found to be less than 150 mg/dL (8.325 mmol/L) in all cases. FDG was injected intravenously (8.7 mCi ± 1.7), and clinical PET imaging began on average 1 hour 19 minutes ± 23 minutes after radiotracer injection. CT examinations were performed after the injection of 150 mL of iohexol (3 mL/sec, Omnipaque 350; GE Healthcare). Whole-body images were reconstructed with contiguous 5-mm section thickness. Dedicated images with 2.5-mm section thickness that covered the lungs were acquired during inspiratory breath hold. These thin-section lung images were used for reference nodule identification and measurement. PET images were obtained with seven to 10 bed positions per patient, with an acquisition time of 3–4 minutes per station, from the skull vertex through the midthigh, without respiratory gating.

PET/MR Imaging Technique

After clinical PET/CT, patients underwent combined PET and MR imaging in a hybrid 3.0-T Signa time-of-flight PET/MR imaging system (GE Healthcare). No additional radiotracer was administered for the PET/MR imaging; the residual activity from the FDG administered for clinical PET/CT scanning was used for the research PET/MR imaging. The time interval from FDG injection to the start of research PET imaging was 2 hours 20 minutes ± 24 minutes. After patient positioning and placement of head-to-thighs radiofrequency surface coil arrays, MR and PET data were acquired concurrently without intravenous contrast material. The MR imaging protocol consisted of a UTE sequence, with the following parameters: repetition time, 2.3 msec; echo time, 80 μsec; flip angle, 4°; 1.25-mm isotropic resolution; adaptive respiratory gating with a 40% acceptance window; and imaging time, 4 minutes 30 seconds (14). A 3D dual-echo GRE sequence with a two-point Dixon method for water-fat separation (LAVA-Flex; GE Healthcare) was performed at end-inspiration with the following parameters: repetition time, 5.6 msec; first echo time, 1.3 msec; second echo time, 2.6 msec; flip angle, 12°; matrix size, 344 × 256; frequency field of view, 42 cm with 80% phase field of view of 2 × 2 Auto-calibrating Reconstruction for Cartesian sampling (GE Healthcare) acceleration; and imaging time, 22 seconds. PET of the lungs was performed with a 12-minute acquisition. No intravenous contrast material was administered for MR imaging. Image quality was good in all cases, and no patients were excluded because of technically insufficient image quality. Imaging parameters for each technique are summarized in Table 2.

Data Collection and Analysis

CT was considered the reference standard for determination of nodule size,

location, and appearance. Nodules were categorized into five subdivisions according to the short-axis dimension by an experienced reviewer (N.S.B., with 7 years of experience) as follows: smaller than 2 mm to smaller than 4 mm, at least 4 mm to smaller than 6 mm, at least 6 mm to smaller than 8 mm, at least 8 mm to smaller than 10 mm, and at least 10 mm. Fissural or pleural nodules and nodules measuring up to 2 mm at CT were not included in the analysis. For each MR imaging technique, assessment of nodule detection and measurement of nodule diameter were repeated by two experienced readers (N.S.B. and T.A.H., who had 10 years of experience) who compared findings with the CT reference standard; mean nodule diameter between readers was used for diameter subgroup classification. In limited cases where there was disagreement between raters regarding nodule detection (three nodules for both UTE and dual-echo GRE imaging), nodules were classified as not detected. In-phase dual-echo GRE series have been reported to be more sensitive for nodule detection compared with "water only" series, and we therefore based our assessment of nodule detection on in-phase images (Fig 1) (2).

Nodule location and FDG avidity were determined by an experienced reviewer (N.S.B.). Nodules were characterized as "central" if they were within 2 cm of hilar structures or "peripheral" if they were within 2 cm of the chest wall or mediastinum. All other nodules were considered "midlung." The "central" definition superseded "peripheral" in cases of group overlap. Nodules were further characterized as "upper lung" if they were located superior to the origin of the upper lobe bronchi and as "lower lung" if they were located inferior to the origin of the basal segmental bronchi. Nodules were defined as subpleural if any margin of the nodule was located within 5 mm of a parietal pleural surface. Nodule FDG avidity was assessed with both clinical PET/CT and PET/MR. FDG avidity was defined as any discernable FDG uptake above background lung activity.

Statistical Analysis

Baseline characteristics are given as means ± standard deviations for continuous variables and frequencies for categorical variables. Comparison of group means was performed with nonparametric Mann-Whitney *U* tests. The χ^2 test and Fisher exact test were used to evaluate differences in frequency of unpaired categorical variables. The McNemar test was used to evaluate paired differences in nodule detection rate between MR imaging techniques. Interrater reliability of nodule detection was determined by means of the unadjusted Cohen κ statistic. Bland-Altman plots were generated to visually depict interrater variance and limits of agreement. All statistical analyses were performed by using Stata version 13.0 software (StataCorp, College Station, Tex).

Results

Nodule Characteristics

The mean number of pulmonary nodules identified per patient with clinical CT was 10.25 ± 11.9 (range, 2–36 nodules; Table 1). The mean nodule diameter at CT was 6.2 mm ± 2.7 (range, 3–17 mm), and most nodules measured up to 1 cm (79 of 82 nodules, 96%). Most nodules were enlarged in size or new compared with findings of prior clinical PET/CT studies (57 of 82 nodules, 70%), but only a minority showed FDG uptake above background on clinical PET/CT images (13 of 82 nodules, 16%). Table 3 presents nodule distribution and characteristics.

Table 3

Nodule Characteristics

Nodule Characteristic:	Value (*n* = 82 nodules)
Mean diameter (mm)*	6.2 ± 2.7
No. of nodules per size category	
>2 to <4 mm	12 (15)
≥4 to <6 mm	28 (34)
≥6 to <8 mm	18 (22)
≥8 to <10 mm	14 (17)
≥10 mm	10 (12)
No. of nodules per craniocaudal location	
Upper	30 (36)
Middle	13 (16)
Lower	39 (48)
No. of nodules per mediolateral location	
Central	26 (32)
Middle	13 (16)
Peripheral	43 (52)
Nodule stability	
Stable	57 (70)
Enlarging or new	25 (30)
Detectable FDG uptake	
None	69 (84)
Positive uptake	13 (16)
Distance from pleura	
<5 mm	35 (43)
≥5 mm	47 (57)
Lobar location	
Right upper lobe	23 (28)
Right middle lobe	7 (8)
Right lower lobe	23 (28)
Left upper lobe	18 (22)
Left lower lobe	14 (17)

Note.—Unless indicated otherwise, data are numbers of nodules with percentages in parentheses.

* Data are the mean ± standard deviation.

Nodule Detection according to Technique

The overall nodule detection rate was 73% (60 of 82 nodules) for UTE sequences and 30% (25 of 82 nodules) for dual-echo GRE sequences ($P < .001$) (Fig 2). The nodule detection rate according to UTE technique was low for nodules larger than 2 mm but smaller than 4 mm in diameter (two of 12 nodules, 17%) but was significantly higher for nodules at least 4 mm in diameter (58 of 70 nodules, 83%; $P < .001$). Similarly, the nodule detection rate with dual-echo GRE imaging was extremely low for nodules larger than 2 mm but smaller than 4 mm in diameter (one of 12 nodules, 8%) but was higher for nodules at least 4 mm in diameter (24 of 70 nodules, 34%), although this did not reach statistical significance ($P = .07$). The nodule detection rate was significantly higher for UTE imaging compared with dual-echo GRE imaging for nodules at least 4 mm in diameter (58 of 70 nodules [83%] vs 24 of 70 nodules [34%], respectively; $P < .001$) and for size categories of at least 4 mm to smaller than 6 mm (71% vs 7%,

Figure 1

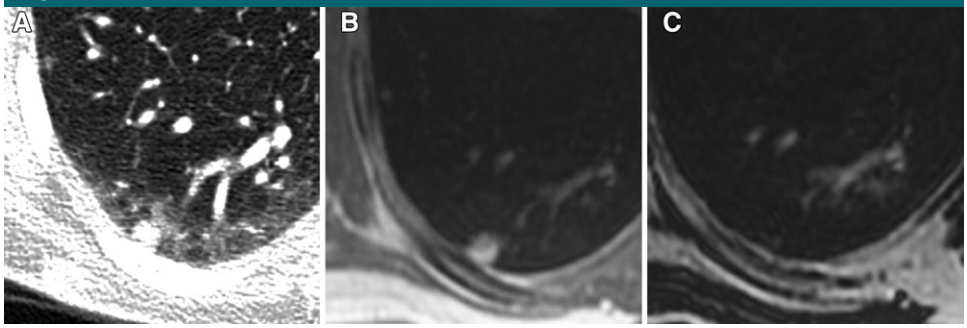

Figure 1: Representative example of a 7-mm subpleural nodule detected on, *A,* a reference axial CT image and, *B,* an axial in-phase MR image; however, it was not detected on, *C,* an axial water-only MR image.

Figure 2

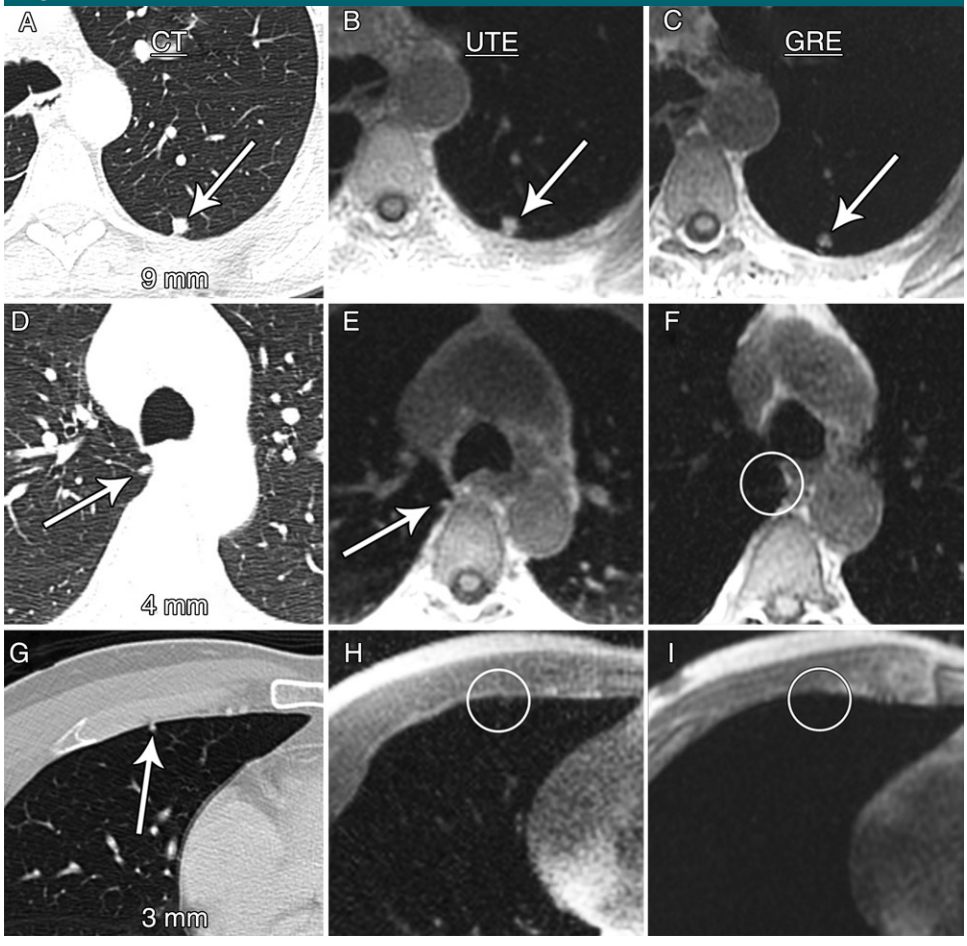

Figure 2: Axial images demonstrate nodule detection with CT (left column), UTE (middle column), and dual-echo GRE (right column) techniques. *A–C,* Nodules larger than 8 mm (arrows) were detected at a high rate with both UTE and GRE MR sequences. *D–F,* The detection rate was significantly lower for dual-echo GRE sequences compared with UTE sequences for nodules at least 4 mm to smaller than 6 mm (arrows on *D* and *E* and circle on *F*). *G–I,* Nodule detection rates for nodules smaller than 4 mm (arrow on *G* and circles on *H* and *I*) were low for both UTE and dual-echo GRE imaging (17% vs 8%, respectively).

Table 4

Nodule Detection Rate according to Lung Imaging Technique

Nodule Characteristic	UTE	Dual-Echo GRE	*P* Value
Size Category			
Overall	60/82 (73)	25/82 (30)	<.001
>2 to <4 mm	2/12 (17)	1/12 (8)	>.99
≥4 to <6 mm	20/28 (71)	2/28 (7)	<.001
≥6 to <8 mm	15/18 (83)	5/18 (28)	.002
≥8 to <10 mm	13/14 (93)	9/14 (64)	.13
≥10 mm	10/10 (100)	8/10 (80)	.5
Detectable FDG uptake			
None	47/69 (68)	15/69 (22)	<.001
Positive uptake	13/13 (100)*	10/13 (77)†	.25
Distance from pleura			
Subpleural (<5 mm)	23/35 (66)	11/35 (31)	.005
Not subpleural (≥5 mm)	37/47 (79)‡	14/47 (30)‡	<.001

Note.—Unless indicated otherwise, data are number of nodules, with percentages in parentheses.

* Statistically significant compared with no detectable FDG uptake (*P* = .02).

† Statistically significant compared with no detectable FDG uptake (*P* < .001).

‡ Not statistically significant compared with subpleural data.

Figure 3

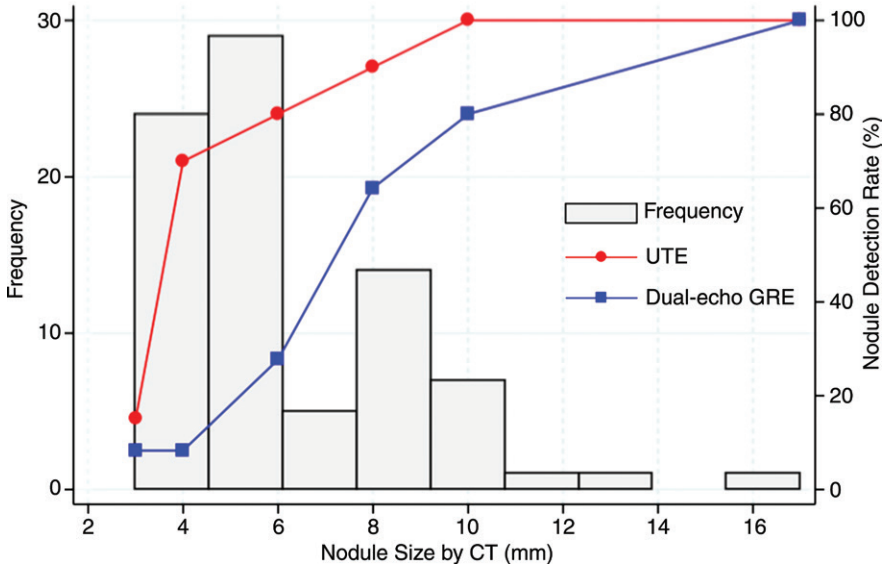

Figure 3: Histogram of nodule diameter as measured with CT with the nodule detection rate by means of imaging technique overlay. The UTE imaging nodule detection rate was significantly higher than that for dual-echo GRE imaging for the size categories of at least 4 mm to smaller than 6 mm (71% vs 7%, respectively; *P* < .001) and at least 6 mm to smaller than 8 mm (83% vs 28%, respectively; *P* = .002).

respectively; *P* < .001) and at least 6 mm to smaller than 8 mm (83% vs 28%, respectively; *P* = .002; Table 4, Fig 3). The nodule detection rate for UTE and dual-echo GRE imaging for nodules 4–8 mm in diameter was 79% (42 of 53 nodules) versus 21% (11 of 53 nodules, *P* < .001). The nodule detection rate did not differ significantly according to patient age or sex.

There was agreement in the assessment of nodule FDG avidity between PET/MR and PET/CT in all cases. FDG-avid nodules were significantly larger than nodules without detectable FDG uptake (9.4 mm ± 3.2 vs 5.6 mm ± 2.1, respectively; *P* = .001). All FDG-avid nodules were detected with UTE sequences (13 of 13 nodules, 100%). The detection rate for FDG-avid nodules with dual-echo GRE imaging was 77% (10 of 13 nodules). The three FDG-avid nodules not detected with dual-echo GRE imaging measured 5 mm, 7 mm, and 10 mm in diameter. FDG-avid nodules were detected at a significantly higher rate compared with nodules without FDG uptake by using both UTE (100% vs 68%, respectively; *P* = .02) and dual-echo GRE (77% vs 22%, respectively; *P* < .001) techniques. UTE sequences had a significantly higher nodule detection rate than dual-echo GRE sequences for nodules without detectable FDG uptake (68% vs 22%, respectively; *P* < .001), particularly among nodules at least 4 mm in diameter (79% [45 of 57 nodules] vs 24% [14 of 57 nodules)], *P* < .001).

Interrater Reliability Analysis

Interrater reliability for the detection of pulmonary nodules was high for both UTE and dual-echo GRE sequences (κ = 0.90 and κ = 0.92, respectively). Interrater reliability for nodule diameter measurements showed a small interrater bias of −0.7 mm ± 1.1 for UTE imaging and 0.2 mm ± 1.2 for dual-echo GRE imaging. Mean rater nodule size measurements from UTE images led to the underestimation of CT measurements by 1.0 mm ± 0.8, whereas mean rater nodule size measurements from dual-echo GRE images led to the underestimation of CT nodule measurements by approximately 0.7 mm ± 1.2. Bland-Altman plots depicting interrater and intermodality agreement are displayed in Figure 4.

Discussion

This pilot study demonstrates that a UTE imaging technique is both feasible and sensitive for the detection of small

Figure 4

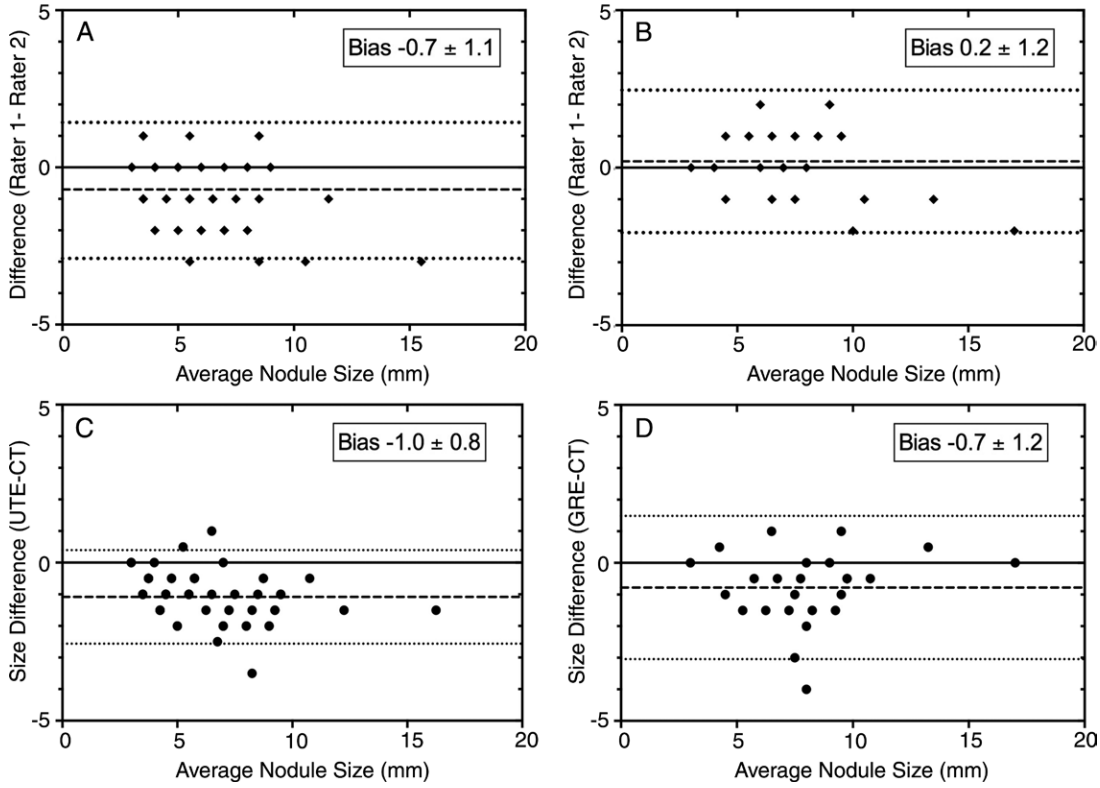

Figure 4: Bland-Altman plots depict interrater reliability and agreement of CT and MR imaging nodule measurements. Small interrater biases were seen fo,r *A,* UTE and, *B,* dual-echo GRE techniques. When compared with reference CT measurements, both, *C,* UTE and, *D,* dual-echo GRE techniques led to underestimation of nodule size by approximately 1 mm.

pulmonary nodules in patients with extrapulmonary malignancies who are undergoing hybrid PET/MR imaging. In such patients, nodules within the 4–8-mm diameter range have a substantial probability of representing metastatic disease, especially when nodules are multiple or when they occur in patients with melanoma, sarcoma, and testicular carcinoma (5,16). In our study, UTE images exhibited an 82% detection rate for pulmonary nodules 4 mm in diameter or larger and outperformed the dual-echo GRE technique for nodule detection in the 4–8-mm range.

Previous studies of MR nodule detection have demonstrated high detection rates for nodules 1 cm in diameter and larger but low detection rates for nodules smaller than 5 mm in diameter (2–4,10,11). Our results largely mirror these findings. Fortunately, such small nodules carry a low risk of malignancy and are particularly low risk when they are located in a subpleural distribution, as were most undetected small nodules in our cohort (5). Similar to other reports, we found that MR imaging techniques led to underestimation of nodule diameter compared with CT, although the intermodality measurement differences we observed were small (1 mm on average) compared with prior reports, in which intermodality measurement differences of 3–4 mm have been described (2).

There are several notable differences between our study and prior studies of pulmonary nodule detection with MR imaging. First, the mean nodule size in our cohort (6 mm) is considerably smaller than that in prior studies, all of which have yielded mean nodule diameters of approximately 1 cm and larger (2–4). While the overall nodule detection rate measured for UTE imaging is comparable to detection rates reported for other MR techniques, the particularly high proportion of subcentimeter nodules in our study suggests a superior performance of UTE imaging for small nodules. Additionally, while our cohort contained a relatively small number of patients, the total number of nodules in our cohort is larger than that in other existing studies. Compared with other MR pulmonary nodule assessment techniques in which breath holds were used, the UTE sequence used in this study was free breathing, thereby decreasing the likelihood of respiratory image degradation in patients who experience dyspnea. Last, for those nodules that exhibited FDG avidity, we did not directly compare quantitative FDG uptake between clinical PET/CT and PET/MR examinations, as other investigators have (3,4), although we noted agreement of FDG

avidity status between modalities for all nodules in the present study. We chose not to compare maximum standardized uptake value calculations between PET/MR and PET/CT because the longer acquisition time and increased detector sensitivity of the PET/MR examination results in lower maximum standardized uptake value calculations, and this difference is dependent on acquisition technique and not modality.

There are several limitations to our study: First, the number of patients in our study was small, although the total number of nodules was relatively large compared with prior studies, owing to the high mean number of nodules per patient. Also, considering that most patients in our cohort had melanoma, we were not able to assess whether nodule detection rates vary by type of primary malignancy, since many common malignancies were either underrepresented or absent in our cohort. Last, the dual-echo GRE technique we used (LAVA-Flex; GE Healthcare) underperformed in the detection of small nodules compared with a recent study in which a similar dual-echo GRE technique was used (3). However, this discrepancy may be due to the fact that mean nodule size and frequency of FDG avidity were substantially lower in our cohort compared with this prior study.

In conclusion, we have demonstrated the feasibility of a free-breathing UTE-based PET/MR lung imaging protocol for the detection of pulmonary nodules. Interrater reliability for nodule detection was high, as was the detection rate for subcentimeter nodules that are large enough to be clinically meaningful. In addition to continued efforts to decrease imaging time and improve small nodule detection, further study is needed to determine the performance of UTE lung imaging in a larger, mixed cohort of oncology patients with varying nodule presence and characteristics.

Disclosures of Conflicts of Interest: N.S.B. disclosed no relevant relationships. **K.M.J.** Activities related to the present article: institution received a grant from GE Healthcare. Activities not related to the present article: disclosed no relevant relationships. Other relationships: disclosed no relevant relationships. **P.E.Z.L.** Activities related to the present article: author received a grant from GE Healthcare. Activities not related to the present article: disclosed no relevant relationships. Other relationships: author has patents and receives royalties from GE Healthcare, Siemens Healthcare, and Philips Healthcare. **M.D.H.** Activities related to the present article: institution received a grant from GE Healthcare. Activities not related to the present article: disclosed no relevant relationships. Other relationships: disclosed no relevant relationships. **S.K.N.** disclosed no relevant relationships. **S.C.B.** Activities related to the present article: author received a grant from General Electric Healthcare. Activities not related to the present article: disclosed no relevant relationships. Other relationships: disclosed no relevant relationships. **T.A.H.** Activities related to the present article: author received a grant from GE Healthcare. Activities not related to the present article: disclosed no relevant relationships. Other relationships: disclosed no relevant relationships.

References

1. Quick HH, von Gall C, Zeilinger M, et al. Integrated whole-body PET/MR hybrid imaging: clinical experience. Invest Radiol 2013;48(5):280–289.
2. Stolzmann P, Veit-Haibach P, Chuck N, et al. Detection rate, location, and size of pulmonary nodules in trimodality PET/CT-MR: comparison of low-dose CT and Dixon-based MR imaging. Invest Radiol 2013;48(5):241–246.
3. Chandarana H, Heacock L, Rakheja R, et al. Pulmonary nodules in patients with primary malignancy: comparison of hybrid PET/MR and PET/CT imaging. Radiology 2013;268(3):874–881.
4. Rauscher I, Eiber M, Fürst S, et al. PET/MR imaging in the detection and characterization of pulmonary lesions: technical and diagnostic evaluation in comparison to PET/CT. J Nucl Med 2014;55(5):724–729.
5. Hanamiya M, Aoki T, Yamashita Y, Kawanami S, Korogi Y. Frequency and significance of pulmonary nodules on thin-section CT in patients with extrapulmonary malignant neoplasms. Eur J Radiol 2012;81(1):152–157.
6. McWilliams A, Tammemagi MC, Mayo JR, et al. Probability of cancer in pulmonary nodules detected on first screening CT. N Engl J Med 2013;369(10):910–919.
7. Khokhar S, Vickers A, Moore MS, Mironov S, Stover DE, Feinstein MB. Significance of non-calcified pulmonary nodules in patients with extrapulmonary cancers. Thorax 2006;61(4):331–336.
8. Quint LE, Park CH, Iannettoni MD. Solitary pulmonary nodules in patients with extrapulmonary neoplasms. Radiology 2000;217(1):257–261.
9. Mayo JR, MacKay A, Müller NL. MR imaging of the lungs: value of short TE spin-echo pulse sequences. AJR Am J Roentgenol 1992;159(5):951–956.
10. Schroeder T, Ruehm SG, Debatin JF, Ladd ME, Barkhausen J, Goehde SC. Detection of pulmonary nodules using a 2D HASTE MR sequence: comparison with MDCT. AJR Am J Roentgenol 2005;185(4):979–984.
11. Regier M, Schwarz D, Henes FO, et al. Diffusion-weighted MR-imaging for the detection of pulmonary nodules at 1.5 Tesla: intraindividual comparison with multidetector computed tomography. J Med Imaging Radiat Oncol 2011;55(3):266–274.
12. Bieri O. Ultra-fast steady state free precession and its application to in vivo (1)H morphological and functional lung imaging at 1.5 tesla. Magn Reson Med 2013;70(3):657–663.
13. Gibiino F, Sacolick L, Menini A, Landini L, Wiesinger F. Free-breathing, zero-TE MR lung imaging. MAGMA 2015;28(3):207–215.
14. Johnson KM, Fain SB, Schiebler ML, Nagle S. Optimized 3D ultrashort echo time pulmonary MRI. Magn Reson Med 2013;70(5):1241–1250.
15. Bergin CJ, Pauly JM, Macovski A. Lung parenchyma: projection reconstruction MR imaging. Radiology 1991;179(3):777–781.
16. Gross BH, Glazer GM, Bookstein FL. Multiple pulmonary nodules detected by computed tomography: diagnostic implications. J Comput Assist Tomogr 1985;9(5):880–885.